Noise estimation in cardiac x-ray imaging: a machine vision approach

Stephen M. Kengyelics[a,*], Amber J. Gislason-Lee[a], Claire Keeble[a], Derek R. Magee[b], Andrew G. Davies[a]

[a] *Division of Biomedical Imaging, Leeds Institute of Cardiovascular and Metabolic Medicine, Worsley Building, University of Leeds, LS2 9JT, United Kingdom*
[b] *School of Computing, EC Stoner Building, University of Leeds, LS2 9JT, United Kingdom*

Abstract

We propose a method to automatically parameterize noise in cardiac x-ray image sequences. The aim was to provide context-sensitive imaging information for use in regulating dose control feedback systems that relates to the experience of human observers. The algorithm locates and measures noise contained in areas of approximately equal signal level. A single noise metric is derived from the dominant noise components based on their magnitude and spatial location in relation to clinically relevant structures. The output of the algorithm was compared to noise and clinical acceptability ratings from 28 observers viewing 40 different cardiac x-ray imaging sequences. Results show good agreement and that the algorithm has the potential to augment existing control strategies to deliver x-ray dose to the patient on an individual basis.

Keywords: x-ray, noise, machine vision, cardiac, imaging

1. Introduction

In this paper, we present a machine vision algorithm to estimate the noise level in real-time cardiac x-ray image sequences. The algorithm has the potential to augment current x-ray dose control strategies to improve the delivery of x-ray images of sufficient quality to accomplish the clinical task and at an x-ray dose to the patient that is more closely matched to the individual procedure.

Cardiovascular Disease (CVD) remains the main cause of death, claiming an estimated 7.4 million lives worldwide in 2012 (World Health Organisation, 2012). Percutaneous coronary intervention (PCI) treats cardiovascular disease that, results in the narrowing of coronary arteries, by improving blood flow to the muscles of the heart. It is a minimally invasive technique that relies on the use of x-ray imaging to capture and display real-time dynamic sequences of coronary arteries (Grech, 2003a,b).

*Corresponding Author
Email address: mrpsmk@leeds.ac.uk (Stephen M. Kengyelics)

PCI procedures may have a number of stages. Initially, clinicians inspect real-time x-ray images of the coronary arteries that are made opaque by the introduction of an iodine-based contrast agent into the vessel lumen. If any significant narrowing is found then an angioplasty may be performed, where a small balloon is positioned in the vessel lumen at the site of the occlusion and expanded to widen it. Often this is followed by deploying a small expandable metal mesh, called a stent, to provide support to the blood vessel and maintain improved blood flow to the heart muscle.

The use of ionizing radiation during these procedures may be a hazard to both patient and staff. Though lowering the radiation dose would be beneficial, any reduction also results in lower quality images that may ultimately compromise patient care. PCI procedures can result in the delivery of high patient dose in comparison with other medical x-ray imaging techniques, due to their complexity, duration, and the need to produce high-quality images (Eisenberg et al., 2011; Žontar et al., 2010; Gislason-Lee et al., 2013). The principle regulating x-ray dose to patients is to reduce it to a level that is as low as reasonably achievable, the so-called ALARA principle, such that the radiation dose is sufficient to achieve the clinical aim. In practice, this level is difficult to establish on an individual basis, as patients differ in body habitus and clinical needs that require the use of a variety of system geometries and x-ray generator settings. In addition, the trade-off between x-ray dose and image quality is dependent on the operating characteristics of the equipment employed.

Currently, the majority of systems regulate their radiation output by seeking to maintain a constant average output signal from the x-ray detector, as illustrated in Fig. 1. Any variations in the imaging field, resulting from a change of view, are compensated for by altering one of the system's variables such as the x-ray tube voltage (kVp), current (mA) or time (ms). The average output from the detector is maintained unless either the system reaches some statutory radiation protection limit, or has insufficient capacity to do so, for example, when imaging a large patient, or employing a steep projection angle. In either case, any further attenuation of the x-ray beam will not result in an increase in the output of the x-ray generator and image noise will increase. This type of automatic dose rate control (ADRC) is implemented in a number of different ways depending on the x-ray equipment vendor and the system mode employed (Lin, 2007, 2009; Lin et al., 2012).

Referring to Fig. 1, for the system used in this study the requested output signal (ROS) is predefined by the vendor and depends on the mode of operation employed. There is little published information on how these baseline predefined levels are established. A recent study demonstrated that it is possible to reduce patient dose by over 30% without affecting the image quality perceived by clinicians viewing angiography image sequences (Gislason-Lee et al., 2015). However, the reduction was not the same for all patients, with a margin of $\pm 15\%$ and only a limited number of cases were considered. This implies there is no single ROS figure that could satisfy a reduction of dose to the patient on a individual level.

In a properly designed x-ray system the predominant source of image noise is

quantum noise. For dynamic real-time imaging quantum noise is both spatially and temporally distributed and the quantum noise power is proportional to the absorbed incident photon fluence and as such does not have a constant value across a typical clinical image, where the attenuation of the patient may change considerably. Therefore, no one single estimate will adequately represent the noise within a clinical image as it is signal-dependent. Most noise measurements in x-ray imaging have focussed on measuring the performance of x-ray image detectors and are based on the measurement of the noise power spectrum (NPS) of flat-field images, that are not modulated by spatially varying signals. These methods are sensitive to trends, or signal content, in the data and require large ensemble averages of noise samples acquired under the same conditions and, therefore, are not suitable to estimating noise across a single clinical image field Kengyelics et al. (1998b,a); Launders et al. (1998); Dobbins III et al. (2006).

In the domain of image processing there have been a large number of noise estimation algorithms developed. The majority of these include one or more common steps that attempt to separate the signal from noise and determine a functional relationship between mean signal and variance. Common stages include the location of homogeneous areas within an image with mean backgrounds that are approximately constant (Salmeri et al., 2001; Shin et al., 2005; Abramov et al., 2008; Uss et al., 2011; Olsen, 1993). In several methods high gradients are detected and excluded from any further analysis. The calculation of variance in these areas is assumed to be an estimate of the noise. Image filtering is used in other methods in an attempt to separate the signal from the background (Liévin et al., 2002; Corner et al., 2003; Russo, 2007; Yang and Tai, 2010; Liu, 2009). Some exploit the difference in spatial scale of the signal and noise in images. Multi-resolution wavelet-based methods generally assume that signal and noise occupy different scales and can be separated into distinct sub-bands (Donoho, 1995; Starck and Murtagh, 1998; De Stefano et al., 2004; Hashemi and Beheshti, 2010). As the separation of signal and noise is often not ideal the distribution of local noise samples will contain outliers. Therefore, some use robust statistical methods to compute the final noise estimates (Alparone et al., 2009; Aja-Fernández et al., 2009; Marais and Steyn, 2009; Ghazal and Amer, 2011). More recently, algorithms have been proposed using principal component analysis (Pyatykh et al., 2013; Pyatykh and Hesser, 2014) and a method that uses arbitrarily large patches of heterogeneous data extracted at random from the image (Azzari and Foi, 2014). In the domain of medical x-ray imaging, where noise is assumed to be heteroscedastic and signal dependent, there have been similar methods developed to separate an estimate of the signal from noise by filtering and the application of robust statistical estimators (Hensel et al., 2006, 2007; Gravel et al., 2004) and to employ wavelet techniques to mammographic images (Salmeri et al., 2008; Mencattini et al., 2008).

Previous attempts to quantify noise in medical images have demonstrated an ability to measure signal dependent noise levels by generating an estimate of the signal by filtering and calculating variance for image regions that have different ranges of mean background level, after excluding high gradient edges from the analysis (Hensel et al., 2006, 2007; Gravel et al., 2004). This was

performed mainly on static images, and the spatial location of the noise was not considered. Clearly when assessed by a human the spatial location within an image is important—high levels of noise around the coronary arteries in a cardiac angiogram would be important, whereas high levels of noise in an area below the diaphragm covered by the spine where there are no arteries of interest has no detriment to the clinical utility of the image.

We propose an approach that considers noise levels in the context of the regions that surround clinically important structures within an image, which in this case were the main coronary arteries. This approach can provide context to the noise measurement to the images. Our method is also designed to work in real time on dynamic image sequences, allowing a changing situation in time to be reacted to for instance as part of a dose control loop. We compared the output of the algorithm with human observer performance and showed that it provides potentially useful information that may be used to augment the existing dose control system in modern cardiac x-ray imaging systems. While a comprehensive quantitative evaluation and validation of the processing steps applied in our proposed method is desirable, this would require a ground-truth, such as a series of clinical images of a subject obtained with different amounts of noise and a detailed knowledge of the underlying anatomical structures. These are not practical to obtain, as it would require multiple x-ray exposures that is hazardous to human health and unethical to perform. Even then it would not be possible to entirely separate quantum noise components from anatomical structure components. Therefore, we tested the approach directly using expert observers operation in an environment that is as close to the clinical setting as practicable and using a threshold contrast detail detectability phantom.

2. Methods

2.1. Description of algorithm

A machine vision algorithm was developed in MATLAB (MATLAB, 2014). The major steps of the algorithm are shown in Table (1) and described below for a single image frame.

1. Extract active image region I_a. The raw data image frames contained dark regions at their periphery produced by the x-ray shuttering employed to limit the irradiation of the patient to areas of clinical interest. There are no useful data in these regions so they were removed before further processing. The shadows of the vertical shutters were identified by averaging pixel values in the vertical direction to form a profile that has a length equal to the width of the image. The profile was smoothed, differentiated, and a threshold was applied to identify the edges of the shutters. The two highest gradients from the profile are generally associated with the shutter edges. Occasionally, this is not true due to structures contained in the image area that also produce high gradients, such as surgical instruments or devices. However, the shutters can be reliably identified as they work as a pair, closing from the periphery of an image to the centre, so spurious edges may

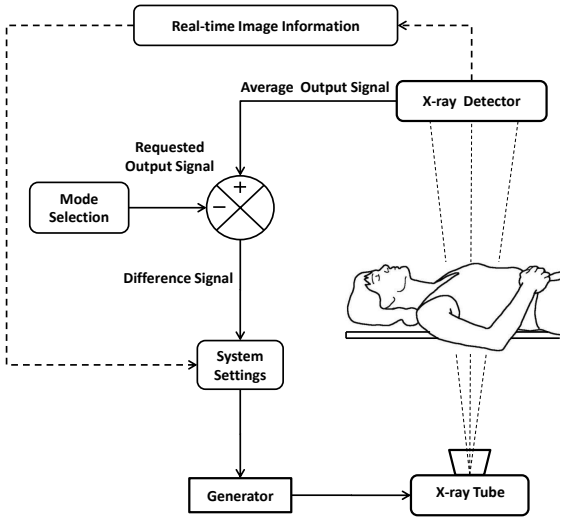

Figure 1: Cardiac x-ray imaging system: Feedback control diagram.

easily be identified. Identification of the horizontal shutters was performed in the same way but in the orthogonal direction. Next the active image area I_a containing the clinically relevant informations was extracted.

2. Estimate image signal I_e from I_a. A median filter with a kernel size of 5 by 5 was applied to I_a to estimate the signal content I_e. The size of the filter was chosen to be the same as Gravel et al. (2004). If the size is too small then the estimate of the signal follows the original too closely and the final estimate of the noise will be underestimated. If it is too large then the influence of edges is increased in areas remote from their location and corrupt the estimate of the local mean. In either case, the separation of signal and noise will not be perfect.
3. Generate mask M_g for high gradient areas in I_e. Areas containing high-gradient features were not included in the analysis of noise because it is difficult to estimate the mean signal in their vicinity. Edges were located by applying a gradient filter to I_e. A mask was constructed from I_e by thresholding the output of the gradient filter such that only the lowest eighth of all the gradients returned were not masked. In this way high-gradient features such as the edges of iodine-filled arteries, or catheters, and other surgical device structures could be excluded from further analysis.
4. Quantize I_a into k levels giving I_k. The pixel values in I_a were mapped uniformly into k levels into an image I_k essentially quantizing the original

Table 1: Noise estimation: List of algorithm steps.

Step	Brief Description
1	Extract active image region $\mathbf{I_a}$
2	Estimate image signal $\mathbf{I_e}$ from $\mathbf{I_a}$
3	Generate mask $\mathbf{M_g}$ for high gradient areas in $\mathbf{I_e}$
4	Quantize $\mathbf{I_a}$ into $\mathbf{k}$ levels giving $\mathbf{I_k}$
5	Generate $\mathbf{k}$ region masks $\mathbf{M_k}$ from $\mathbf{I_k}$ from largest connected area at each level
6	Generate noise image $\mathbf{I_n} = \mathbf{I_a} - \mathbf{I_e}$
7	Calculate noise $\mathbf{N_k}$ from $\mathbf{I_n}$ for each region $\mathbf{M_k}$ excluding $\mathbf{M_g}$.
8	Aggregate $\mathbf{N_k}$ into a single noise measure.

image to produce a new image whose values were the indices of the range of pixel values contained in the original. For the purposes of this study k was chosen to be 4, but could be higher if a more detail spatial distribution of variance is required. The images were had 8-bit bit depth.

5. Generate k region masks M_k from I_k from the largest connected area at each level. A set of binary masks M_k were generated from the quantized image I_k for each level k. Each mask was produced from the largest connected area at each level as this was, in practice, sufficient to cover the majority of the image area across k levels.
6. Generate noise image $I_n = I_a$ - I_e. The influence of background structures was suppressed by subtracting the signal estimate image from the original image.
7. Calculate noise N_k from I_n for each region M_k, excluding M_g. For each slice level k the noise was estimated by calculating the variance in I_n for the region delineated by M_k, but excluding the high-gradient regions defined by M_g.
8. Aggregate N_k to a single metric. The regions represented by M_k that overlay the major iodine-filled coronary arteries are located by comparing the coordinates of the points contained within each boundary to those of the center-lines of the vessels. The center-lines of the vessels are supplied from an algorithm developed in a previous study (Kengyelics et al., 2015). If one or more of the M_k boundaries overlays the coronaries a mean score is calculated from the corresponding values of N_k and scaled to the proportion of total area occupied and then returned. In the case of a sequence of images the score is averaged for the previous 10 frames. Therefore, the algorithm gives an aggregate noise measurement in regions surrounding the location of the main coronary arteries, which are the structures of interest in the clinical image.

2.2. Clinical image sequence acquisitions

Twenty clinical PCI image sequences were obtained from a modern flat-panel x-ray imaging system operating in the Leeds General Infirmary, United Kingdom, (Allura Xper FD10, Philips Healthcare). A propriety data capture device installed by the manufacturer was used to acquire image data prior to the application of any complex non-linear image processing algorithms during routine PCI procedures. The effect of specific image processing algorithms were not considered in this study. The operation of such algorithms vary considerably between equipment manufactures and even amongst applications settings on single systems. The only processing applied to the data prior to capture was linear scaling and a dynamic range compression look-up table and, therefore, the results of this study are generalizable.

Each test sequence contained approximately 30-50 image frames of 1024 × 1024 pixels with 16-bit depth, of which 10-bits are used. For this study the images were converted to 8-bit images. The patient images did not contain any personal information and their use for this study was approved by the National Health Service Research Ethics Committee.

Clinical images were selected from different patient examinations, and comprised 10 left coronary artery (LCA) and 10 right coronary artery (RCA) sequences, acquired at 15 frames per second, using the digital-acquisition (cine) mode and 15 cm field size. The image sequences chosen did not contain any additional catheters, guide wires or other surgical devices other than the main catheter used to introduce the iodine contrast agent. Summary information for the image sequences is shown in Table 2.

Table 2: Images Sequence Summary Information

	Minimum	**Maximum**	**Mean**	**Standard Deviation**
X-ray Tube Voltage(kVp)	70.1	121.4	83.6	12.1
X-ray Tube Current(mA)	588.8	921.9	816.8	96.2
X-ray Tube Pulsewidth(mS)	5.2	9.9	7.1	1.1
Angulation (Degrees)	-27.5	28.1	5.4	19.3
Rotation (Degrees)	-34.1	35.8	-8.7	24.0
Source-to-Detector Distance(cm)	103.1	121.0	113.6	4.7
Table Height (cm)	89.8	105.2	98.7	3.2

2.3. Test image synthesis

Further test images were generated from the originals by adding noise to simulate acquiring a sequence at a lower x-ray dose. Dose reduction levels were randomly generated between 20–75%. One test sequence was generated per original, with a randomly allocated dose reduction factor, making a total of 40 sequences. The methodology used has been previously validated and reported by Gislason-Lee et al. (2015).

2.4. Observer study

Twenty-eight observers viewed the images, graded their clinical acceptability, and rated their level of noise. Images were viewed on a high-quality medical-grade viewing monitor (RadiForce RX340, EIZO Corporation, Ishikawa, Japan). The monitor was DICOM-calibrated to proved a perceptually linear response. The observers comprised various professions having different levels of experience viewing cardic PCI image sequences as summarised in Table 3. The sequences were viewed at 15 frames per second using 8-bit depth presentation. The observers were asked to view each image sequence and rate the level of noise on a continuous scale displayed on the bottom of the viewing area, graded from *negligible* to *very noisy* produced a value between zero and one. Observers were also asked to decide if the image sequence was *satisfactory* or *unsatisfactory* to be able to determine the presence and severity of stenotic lesions. Each of the two types of questions was asked independently and sequences were presented at random i.e. the two types of question were made by separate presentations of the same sequence that were not presented sequentially.

2.5. Threshold Contrast Detail Detectability

Images were acquired of a commercially available test object TO10 (Leeds Test Objects, Boroughbridge, North Yorkshire) as shown in Fig. 2. The test object was imaged at 75 kVp, with 2.5 mm Cu additional filtration, and the mAs adjusted to give a range of detector entrance surface doses, viz. 16, 36, 54, 85 and 101 nGy/frame. The scoring of the test object was performed following the methods of Launders et al. (1995). Briefly, three images at each dose were viewed by three experienced observers on a medical grade computer monitor in dimmed ambient lighting conditions. The number of disks visible in each observation were converted into contrast thresholds, and then averaged to produce a threshold per disk size for each dose. We compared the averaged detection index $H_T(A)$ for rows 4–7 (disk radii of 1.1, 0.9, 0.8 and 0.6 mm), to the noise estimate from the new algorithm. $H_T(A)$ is calculated according to $1/C_T(A)$, where C_T is the threshold contrast and A the area of the detail.

3. Results and discussion

Some of the following results are provided to illustrate the output of the algorithm, but are generally applicable for all of the image sequences examined in this study unless otherwise stated.

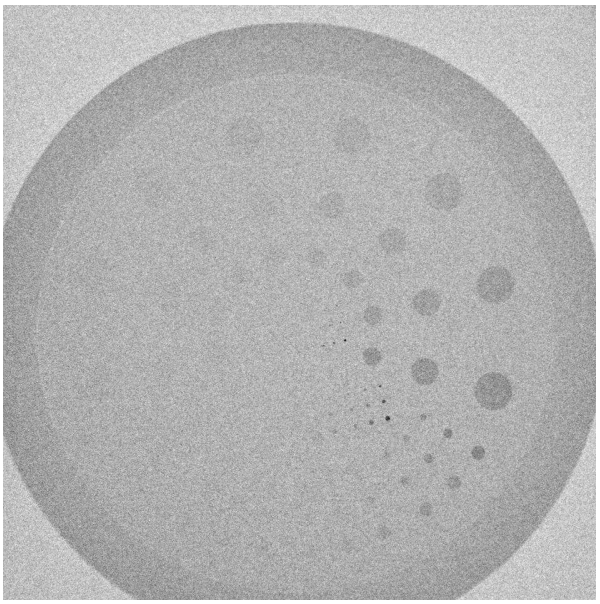

Figure 2: Threshold Contrast Detail Detectability Test Object.

Figure 3 shows a single frame from a PCI LCA sequence with the coronary arteries filled with contrast medium, together with a color-coded variance map calculated by the algorithm. The variance map includes the outline of the mask used to exclude features with high gradients. The same image frame is shown at two further simulated dose levels decreasing from left to right. Note how the visual impression of noise is reflected in the corresponding variance map. This figure illustrates that the noise contained in a typical PCI image frame may be subdivided into a small finite number of regions that give good coverage across the image. For the purposes of illustration the figure shows all the regions calculated within a specified signal range and not just the largest area. Figure 4 shows an example of choosing just the largest areas calculated by the algorithm at each of the four output levels.

Figure 5 shows the calculated variance for each of the four areas highlighted in Figure 4 as a function of percentage dose reduction. Note that there is over an order of magnitude difference between the lowest and highest variance values.

In Figure 6 variance is plotted as a function of time indicated by the frame number. The estimate of variance appears relatively stable with time despite the dynamic content of the image, apart from for level 1. This is due to the relatively small area of the corresponding variance map and its location that is associated with contrast media escaping from the coronary artery ostia into the aorta. This process is not stable with time as reflected in the variance map at this signal level. The figure demonstrates that the algorithm is insensitive to

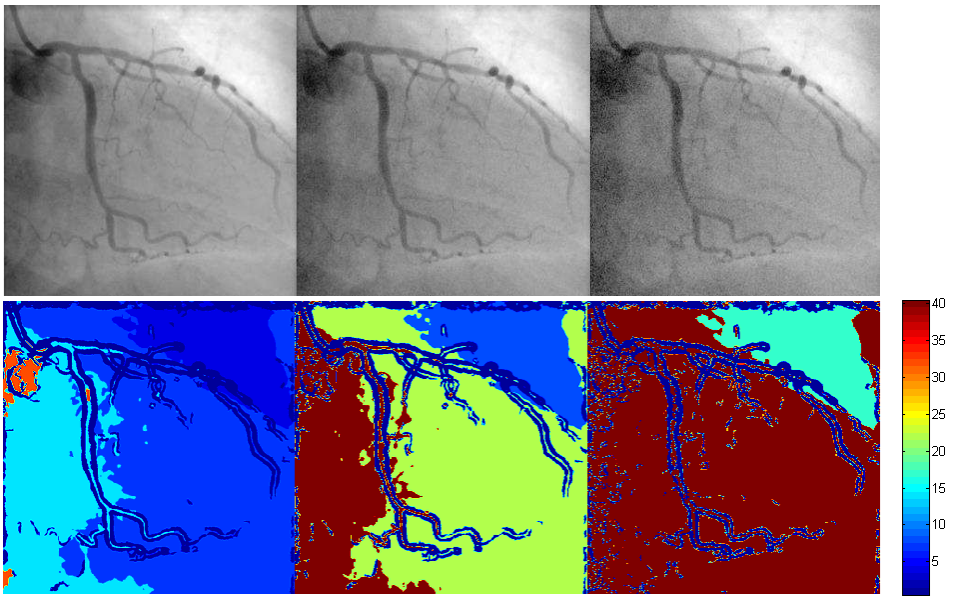

Figure 3: PCI LCA Image frame: (left to right) 0, 25, 50% dose reduction (top) and corresponding variance maps below.

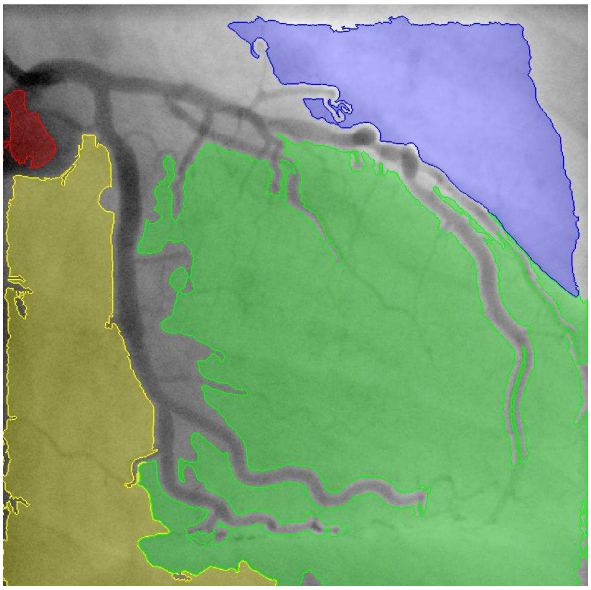

Figure 4: PCI LCA image frame showing location of variance map overlays (colors denote variance as in Figure 2).

Table 3: Observer Summary Statistics

Profession	**Number of Observers**	**Experience Range** (Years)	**Experience Mean** (Years)
Interventional Cardiologist	7	5-37	16.4
Cardiologist Registrar	5	1-7	3.4
Radiographer	8	4-30	15.1
Medical Physicist	6	1-30	16.3
Nurse	1	9	9
Other	1	1	1

the inflow and outflow of the contrast media in the vessels and the motion of the heart for levels 2–4.

Figure 7 shows the percentage area of each of the four output levels for the image sequence shown in Figure 6. Level 1 is the smallest of the areas, so despite its temporal instability and high variance compared to the other levels, it has little impact on the overall image. The variation in the percentage area at all levels reflects the change of size of the variance maps due to patient movement and the inflow and outflow of the contrast media.

Figure 8 shows the observed mean noise rating of the 28 observers for each image sequence against the value returned from the algorithm. The sequences that were judged to be clinically inadequate by more than 50% of the observers are indicated as unacceptable. The figure demonstrates the importance of noise for an observer judging the clinically acceptable image as might be expected. In addition, by setting a suitable threshold for the measured variance metric there is a reasonable separation of the two classes of acceptable and unacceptable images. Further work is required to establish a suitable threshold that would be applicable to a broader population of patients and range of examinations than was possible in this limited study.

Figure 9 shows the detection index $H_t(A)$ against the measured variance indicating that observer performance increases with decreasing variance. In other words, observer performance and measured noise are improved with an increase in detector dose. This confirms the ability of the algorithm to reflect a change in observer performance with respect to a detection task.

4. Conclusion

We have developed an automatic machine vision algorithm to measure noise in PCI cardiac image sequences. The measurement algorithm may be useful in an ADRC scheme that monitors noise that is significant with respect to how human observers rate the clinical acceptability of images and seeks to reduce it. It may also be useful in a post acquisition quality assurance scheme to analyse image sequences to ensure inter and intra system consistency. The overall aim

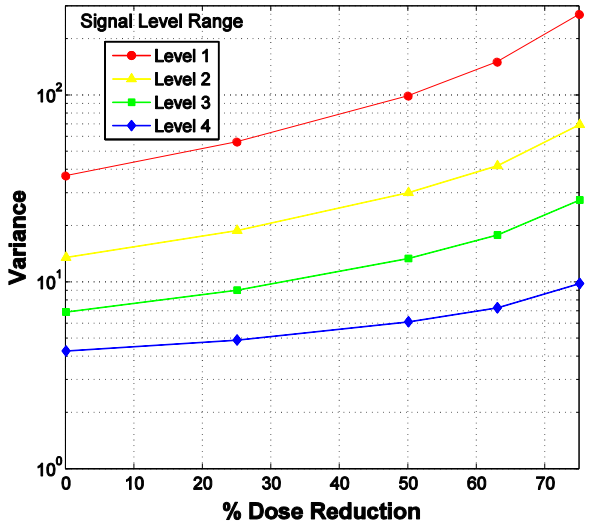

Figure 5: Variance vs. percentage dose reduction for the PCI LCA image frame shown in Figure 4.

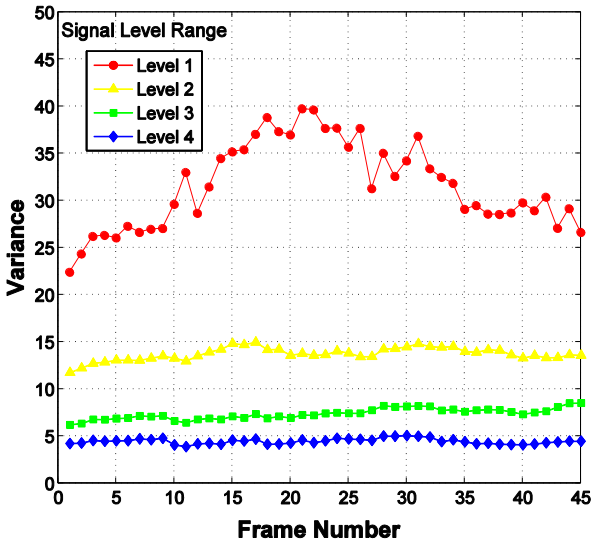

Figure 6: Variance vs. frame number (15 frames per second, No dose reduction).

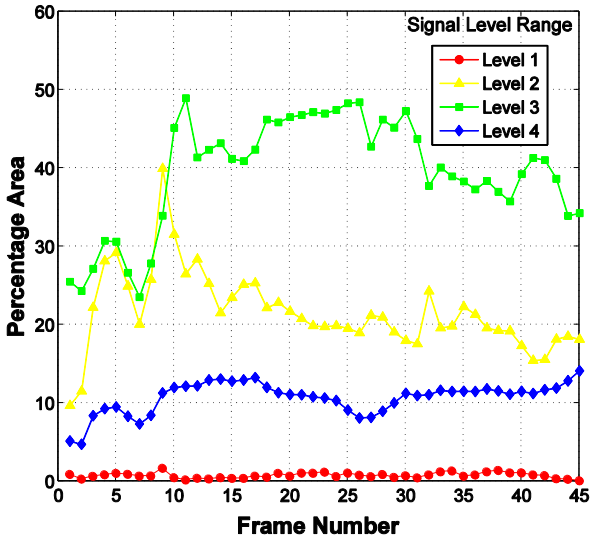

Figure 7: Percentage area vs. frame number (15 frames per second)

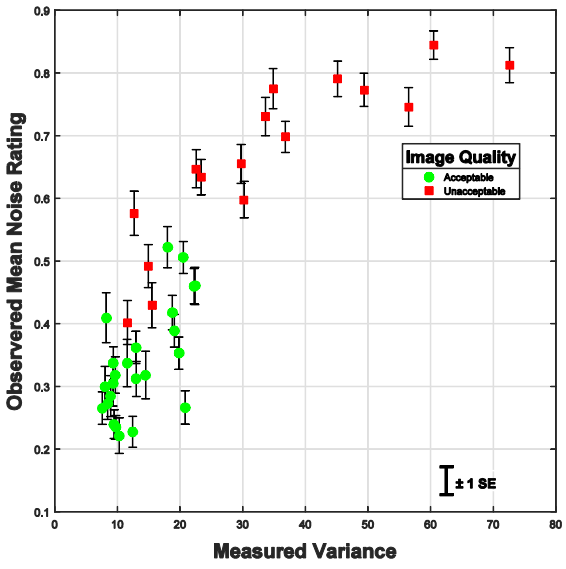

Figure 8: Observed mean noise rating vs. measured variance. 28 observers, 40 images. Unacceptability based on greater than 50% of observers agreeing.

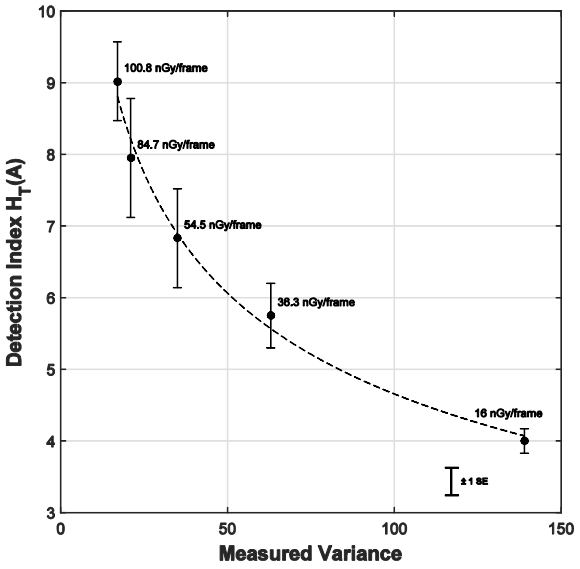

Figure 9: Detection index vs measured variance. Three observers. Text labels denote entrance surface dose to the detector.

was to provide context-sensitive imaging information for use in the dose control feedback system that relates to observer experience. Noise is not the only important aspect of image quality for cardiac imaging. Contrast, spatio-temporal resolution properties, and the application of specialist image processing are also critically important. We selected noise for this investigation, as the x-ray imaging system has a convenient means of influencing it by setting a requested output signal (ROS) for the x-ray detector. The results show good correspondence between average observer noise rating and the level of noise measured in key areas within the image by the machine algorithm. Low levels of measured noise were predictive of improved observer performance in a detection task. The study was limited to image sequences that did not contain any additional catheters, guide wires or other surgical devices other than the main catheter used to introduce the iodine contrast agent.

Future work will focus on excluding these structures from the variance measurement, on the implementation of the algorithm in a practical dose control system, and establishing suitable image quality thresholds across a much wider population than was possible in this study.

Acknowledgements

This work has been performed in the project PANORAMA, funded by grants from Belgium, Italy, France, the Netherlands, United Kingdom, and the ENIAC

Joint Undertaking.

References

Abramov, S. K., Lukin, V. V., Vozel, B., Chehdi, K., Astola, J. T., 2008. Segmentation-based method for blind evaluation of noise variance in images. Journal of Applied Remote Sensing 2 (1), 023533–023533.

Aja-Fernández, S., Vegas-Sánchez-Ferrero, G., Martín-Fernández, M., Alberola-López, C., 2009. Automatic noise estimation in images using local statistics. additive and multiplicative cases. Image and Vision Computing 27 (6), 756–770.

Alparone, L., Selva, M., Capobianco, L., Moretti, S., Chiarantini, L., Butera, F., 2009. Quality assessment of data products from a new generation airborne imaging spectrometer. In: Geoscience and Remote Sensing Symposium, 2009 IEEE International, IGARSS 2009. Vol. 4. IEEE, pp. IV–422.

Azzari, L., Foi, A., 2014. Indirect estimation of signal-dependent noise with nonadaptive heterogeneous samples. IEEE Transactions on Image Processing 23(8), 3459–3467.

Corner, B., Narayanan, R., Reichenbach, S., 2003. Noise estimation in remote sensing imagery using data masking. International Journal of Remote Sensing 24 (4), 689–702.

De Stefano, A., White, P., Collis, W., 2004. Training methods for image noise level estimation on wavelet components. EURASIP Journal on Applied Signal Processing 2004, 2400–2407.

Dobbins III, J. T., Samei, E., Ranger, N. T., Chen, Y., 2006. Intercomparison of methods for image quality characterization. II. Noise power spectrum. Medical Physics 33, 1446–1576.

Donoho, D. L., 1995. De-noising by soft-thresholding. Information Theory, IEEE Transactions on 41 (3), 613–627.

Eisenberg, M. J., Afilalo, J., Lawler, P. R., Abrahamowicz, M., Richard, H., Pilote, L., 2011. Cancer risk related to low-dose ionizing radiation from cardiac imaging in patients after acute myocardial infarction. Canadian Medical Association Journal 183(4), 430–436.

Ghazal, M., Amer, A., 2011. Homogeneity localization using particle filters with application to noise estimation. Image Processing, IEEE Transactions on 20 (7), 1788–1796.

Gislason-Lee, A. J., Kumcu, A., Kengyelics, S. M., Brettle, D. S., Treadgold, L. A., Sivananthan, M., Davies, A. G., 2015. How much image noise can be added in cardiac x-ray imaging without loss in perceived image quality?

Journal of Electronic Imaging 24 (5), 051006.
URL http://dx.doi.org/10.1117/1.JEI.24.5.051006

Gislason-Lee, A. J., McMillan, C., Cowen, A. R., Davies, A. G., 2013. Dose optimization in cardiac x-ray imaging. Medical Physics 40, 091911–1–11.

Gravel, P., Beaudoin, G., De Guise, J., et al., 2004. A method for modeling noise in medical images. Medical Imaging, IEEE Transactions on 23 (10), 1221–1232.

Grech, E., 2003a. Percutaneous coronary intervention. I. History and development. British Medical Journal 326, 1080–1082.

Grech, E., 2003b. Percutaneous coronary intervention. II. The procedure. British Medical Journal 326, 1137–1140.

Hashemi, M., Beheshti, S., 2010. Adaptive noise variance estimation in bayesshrink. IEEE Signal Processing Letters 1 (17), 12–15.

Hensel, M., Lundt, B., Pralow, T., Grigat, R.-R., 2006. Robust and fast estimation of signal-dependent noise in medical x-ray image sequences. In: Bildverarbeitung für die Medizin 2006. Springer, pp. 46–50.

Hensel, M., Pralow, T., Grigat, R.-R., 2007. Modeling and real-time estimation of signal-dependent noise in quantum-limited imaging. In: Proceedings of the 6th WSEAS international conference on signal processing, robotics and automation, Corfu Island, Greece, ACM Proceedings. pp. 183–191.

Kengyelics, S. M., Davies, A. G., Cowen, A. R., 1998a. A comparison of the physical imaging properties of Fuji ST-V, ST-VA and ST-VN computed radiography image plates. Medical Physics 25, 2163–2169.

Kengyelics, S. M., Gislason-Lee, A. J., Keeble, C., Magee, D. R., Davies, A. G., 2015. Context sensitive cardiac x-ray imaging: a machine vision approach to x-ray dose control. Journal of Electronic Imaging 24 (5), 051002–051002.

Kengyelics, S. M., Launders, J. H., Cowen, A. R., 1998b. Physical imaging performance of a compact computed radiography acquisition device. Medical Physics 25 (3), 354–360.

Launders, J., Kengyelics, S., Cowen, A., 1998. A comprehensive physical image quality evaluation of a selenium based digital x-ray imaging system for thorax radiography. Medical physics 25 (6), 986–997.

Launders, J. H., Mcardle, S., Workman, A., Cowen, A. R., 1995. Update on the recommended viewing protocol for faxil threshold contrast-detail detectability test objects used in television fluoroscopy. British Journal of Radiology 68 (805), 70–77.

Liévin, M., Luthon, F., Keeve, E., 2002. Entropic estimation of noise for medical volume restoration. In: Pattern Recognition, 2002. Proceedings. 16th International Conference on. Vol. 3. IEEE, pp. 871–874.

Lin, P. P., 2007. The operation logic of automatic dose control of fluoroscopy system in conjunction with spectral shaping filters. Med. Phys. 34 (8), 3169–3172.

Lin, P. P., 2009. Operation logic and functionality of automatic dose rate and image quality control of conventional fluoroscopy. Med. Phys. 36 (5), 1486–1493.

Lin, P. P., Rauch, P., Balter, S., Fukuda, A., Goode, A., Hartwell, G., LaFrance, T., Nickoloff, E., Shepard, J., Strauss, K., 2012. Functionality and operation of fluoroscopic automatic brightness control/automatic dose rate control logic in modern cardiovascular and interventional angiography systems: A report of Task Group 125 Radiography/Fluoroscopy Subcommittee, Imaging Physics Committee, Science Council. AAPM Report 125.

Liu, A., 2009. A fast method of estimating gaussian noise. In: The 1st International Conference on Information Science and Engineering (ICISE). IEEE, pp. 441–444.

Marais, I. Z., Steyn, W., 2009. Noise estimation algorithms for onboard image quality assessment. In: International Conference on Space Technology.

MATLAB, 2014. Version 8.3.0.532 (R2014a). The MathWorks Inc., Natick, Massachusetts.

Mencattini, A., Salmeri, M., Lojacono, R., Frigerio, M., Caselli, F., 2008. Mammographic images enhancement and denoising for breast cancer detection using dyadic wavelet processing. IEEE Transactions on Instrumentation and Measurement, 57 (7), 1422–1430.

Olsen, S. I., 1993. Estimation of noise in images: an evaluation. CVGIP: Graphical Models and Image Processing 55 (4), 319–323.

Pyatykh, S., Hesser, J., 2014. Image sensor noise parameter estimation by variance stabilization and normality assessment. Image Processing, IEEE Transactions on 23 (9), 3990–3998.

Pyatykh, S., Hesser, J., Zheng, L., 2013. Image noise level estimation by principal component analysis. Image Processing, IEEE Transactions on 22 (2), 687–699.

Russo, F., 2007. Gaussian noise estimation in digital images using nonlinear sharpening and genetic optimization. In: Instrumentation and Measurement Technology Conference Proceedings IMTC 2007. IEEE, pp. 1–5.